Chapter 5

Long Term Evolution of The Jet

5.1 Introduction

In this chapter, we discuss the long–term evolution of the radio emission coming from the parsec–scale regions in 3C 345. We describe changes of the component emission at 5, 8–11, and 22 GHz. The data at 8 and 11 GHz are combined together, because of relative closeness of the frequencies, and because of insufficient time coverage at each of them. Most of the 11 GHz observations were made before 1990; later the observing frequency was changed to 8 GHz, for this part of spectrum.

Flux variations at different frequencies reflect both intrinsic evolution of component emission and changes of the optical depth in the ambient media. Patterns of flux variability observed at lower frequencies are expected to be delayed, with respect to the corresponding events observed at higher frequencies; this effect has been observed in total flux monitoring programs (Lainela *et al.* 1991). In this chapter, we examine the fluxes of parsec–scale features, in a search for similar behavior.

Using the results of fitting synchrotron spectrum (see Section 4.3), we study changes of the component spectra and luminosities. The luminosity evolution of different components are compared with the kinematic parameters, in order to find possible correlations and make conclusions about the jet physics.

5.2 Flux evolution

The fluxes of the core and all jet components (except C1 for which there are too few detections available) are plotted in Figures 5.1–5.4. The jet components are covered by the flux measurements unequally, depending on the component separation, spectrum and brightness. For the older components C2, and C3, there are no detections at 22 GHz. Contrary to that, the youngest component, C7, has been detected at 22 GHz predominantly. The components with the most complete flux curves in the overall data are D, C5, and C4.

5.2.1 Maximum flux at different frequencies

The delay of flux maximum at lower frequencies is seen in the core, although a possibility of confusion cannot be excluded, because of the sparsity of observation epochs. The delay can also be guessed from the flux rise seen in C7 at 5 and 8 GHz, after the component reached its maximum at 22 GHz (see Figure 5.1). There is no apparent delay of flux maximum in the flux curves of C5 (Figure 5.2) and C4 (Figure 5.3). Frequency dependence of the optical depth expected in the proximity of the core (Blandford & Königl 1979) can explain why the delay is not seen at larger separations from the core (fluxes of C4 and C5 reached their maxima at ≈1 mas distance from the core, while the maximum 22 GHz flux of C7 occured at ≈0.3 mas).

5.2.2 Core and strong jet components

The flux changes of the core and the jet components close to the core are more profound compared to the flux evolution observed at larger separations from the core. The 5 GHz fluxes of the core and C4, and C3 decrease at the rate of about 15% a year (for C4 and C3 the rate is measured for separations from 1 to 2 mas from the core). As the components move farther away from the core, the decrease rate becomes smaller (about 6% a year for C3 and C2; nearly constant for C4). This indicate that there may be a mechanism that slows down or even neutralizes the energy losses, at larger separations from the core. One of the possible explanations is increasing Doppler boosting. The Doppler boosting increase may be caused by variations of the jet viewing angle, as well as by reacceleration due to plasma interactions in the jet.

Similar changes of the flux decrease rate are observed in C4, and C3 at 8 GHz. This suggests that the effect is likely to reflect changes of kinematical or physical conditions of the jet.

5.2.3 C5 and C6

Both C5 and C6 have peculiar flux evolutions, making them outstanding jet features. At all three frequencies, the flux of C5 rises more slowly than the fluxes of C4 and C7. The decrease of flux varies significantly in C5. The 5 GHz flux decreases by ≈17% a year, from 1988 to 1994. At the same time the fluxes at 8 and 22 GHz drops in 1988 by 80% and 65% respectively. Subsequently, the 5 and 8 GHz fluxes of C5 decline by about 5% a year.

The peculiarity of C6 is reflected in the extremely low 22 GHz flux of the component ($S_{C6} < 0.3$ Jy). C6 becomes undetectable in 22 GHz images, at 1 mas separation. C4 and C5 were at their maxima, at comparable separations; C7 had passed its maximum, but still was much stronger. The unusual flux evolution of C6 may be related to its peculiar kinematical evolution.

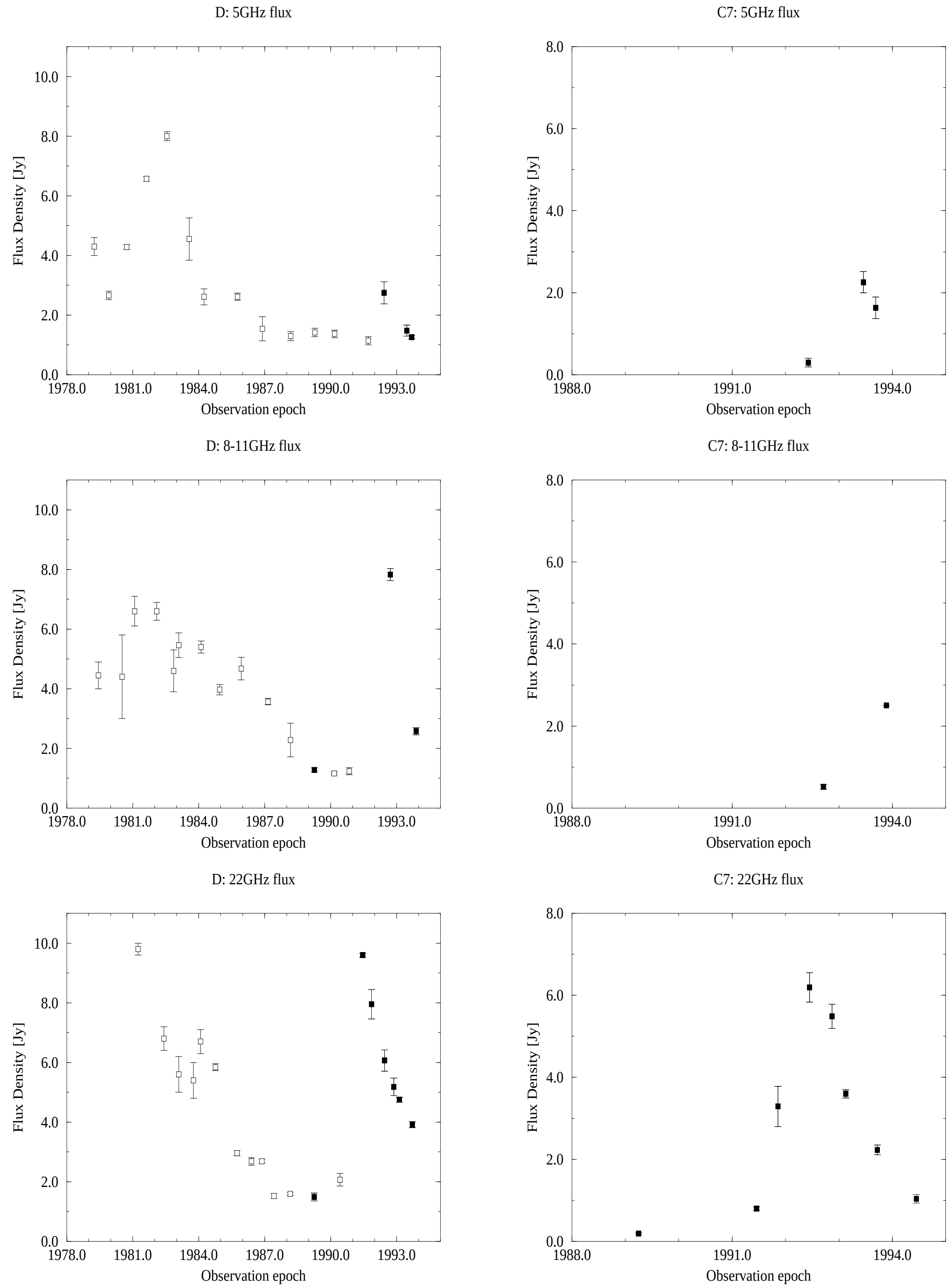

Figure 5.1: 5, and 8 GHz flux evolution of D (left column) and C7 (right column). Filled squares indicate the data from this thesis.

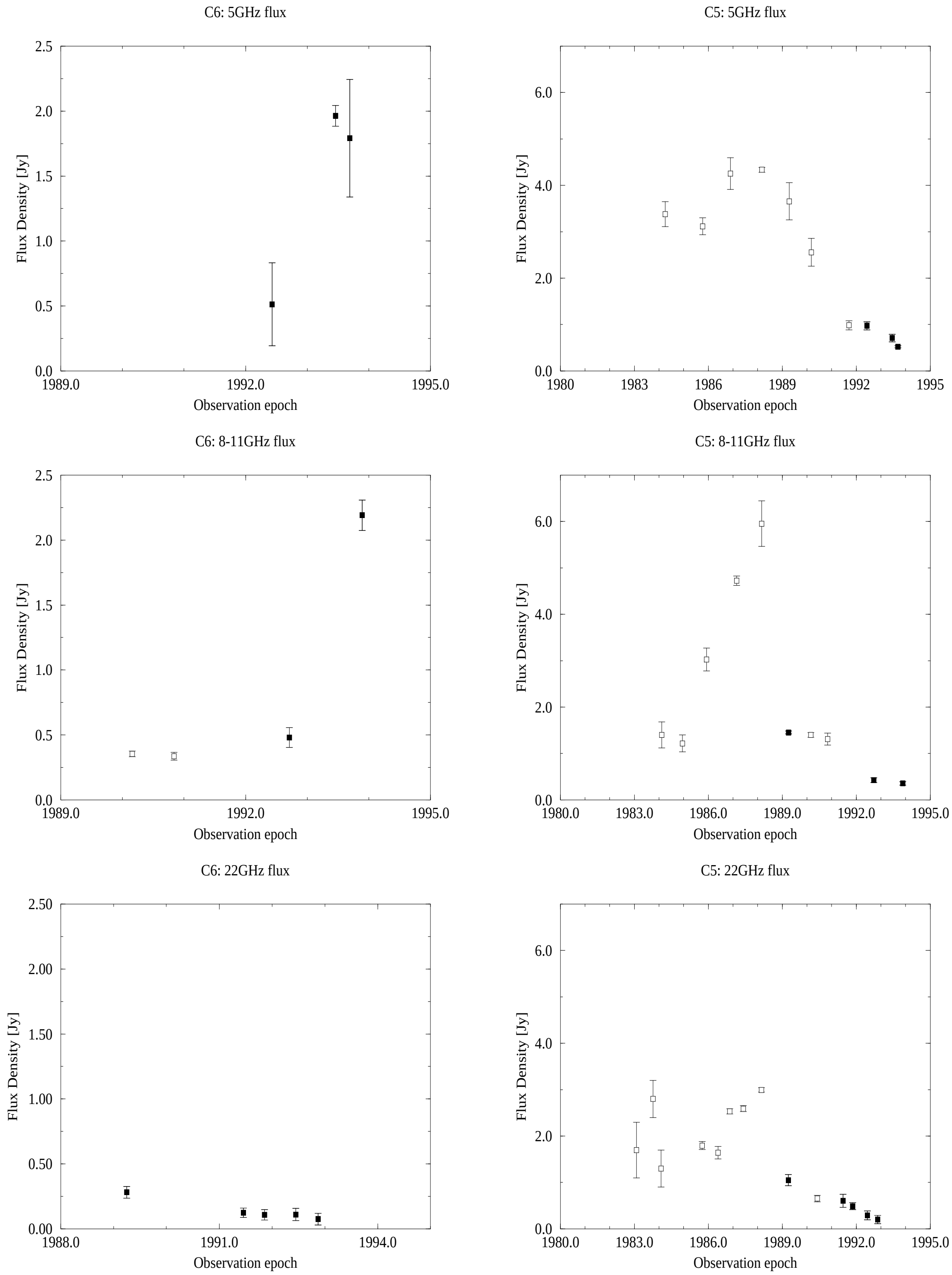

Figure 5.2: 5, 8, and 22 GHz flux evolution of C6 (left column) and C5 (right column). Filled squares indicate the data from this thesis.

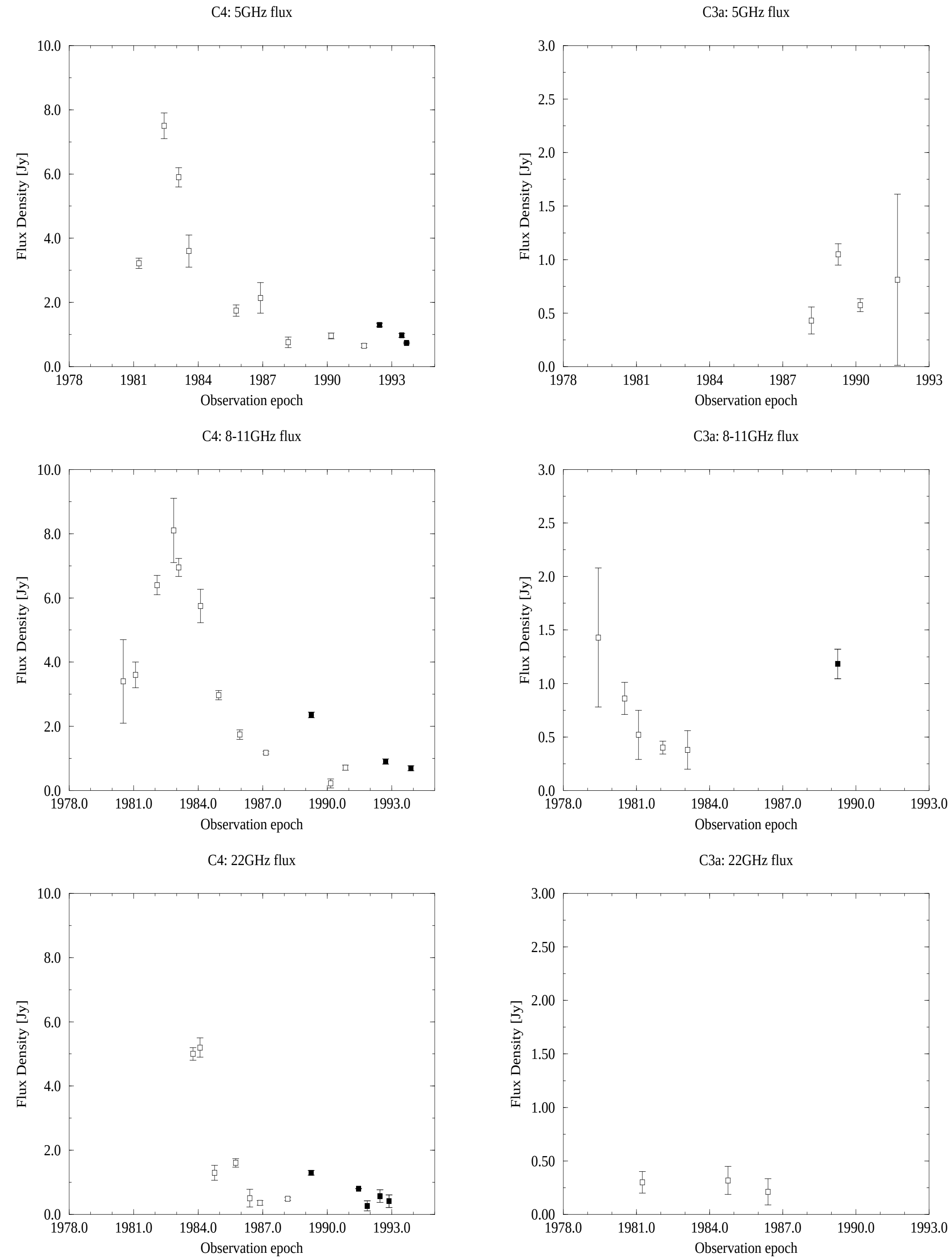

Figure 5.3: 5, 8 and 22 GHz flux evolution of C4 (left column) and C3a (right column). Filled squares indicate the data from this thesis.

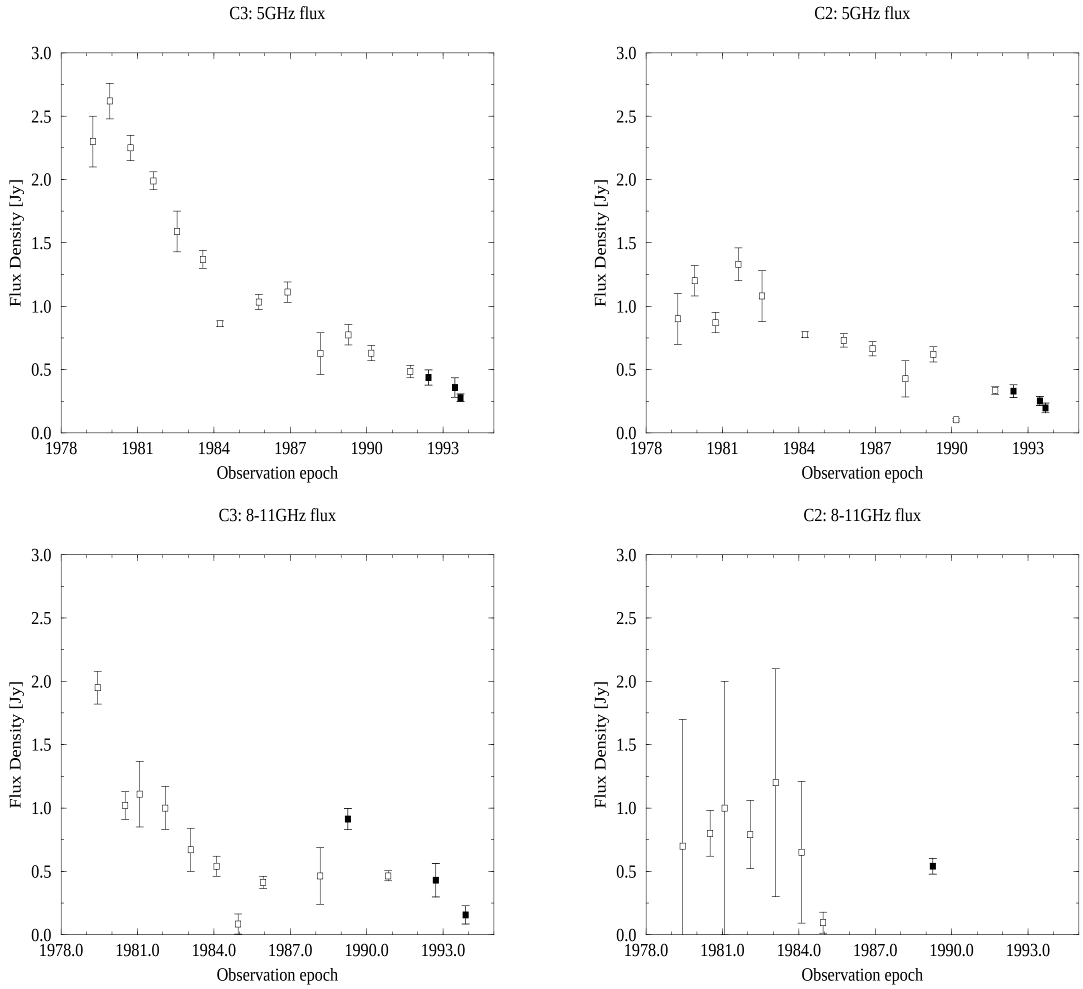

Figure 5.4: 5, and 8 GHz flux evolution of C3 (left column) and C2 (right column). Filled squares indicate the data from this thesis.

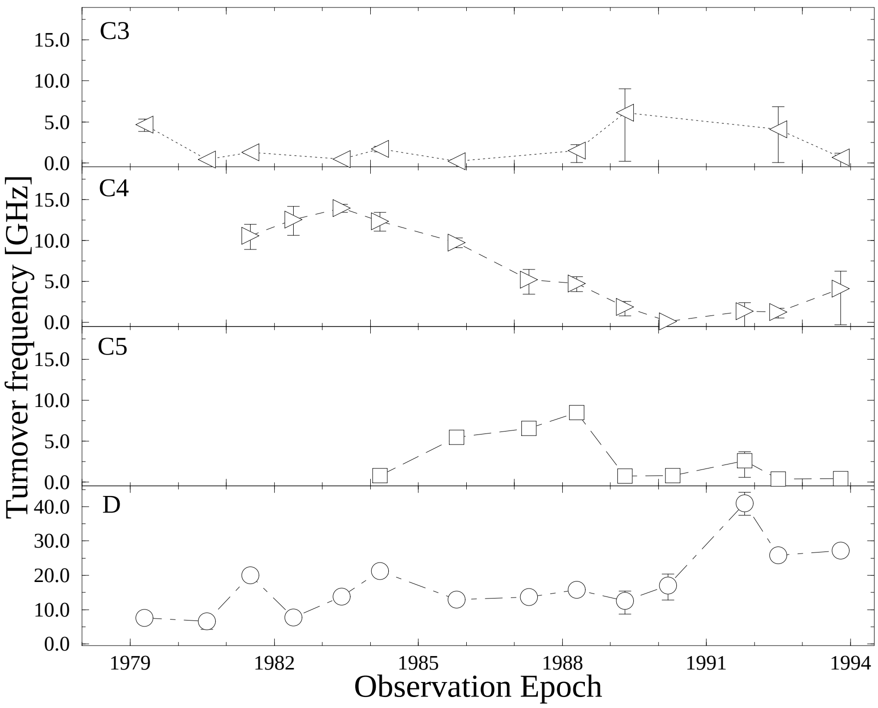

Figure 5.5: Evolution of the turnover frequency ν_m in the core and the jet components of 3C345.

5.3 Spectral properties of the jet components

In this section, we discuss the relationships between the derived spectral parameters of the jet components. The spectral information is then combined with the observed kinematic properties of the components, to study the luminosity evolution.

5.3.1 Evolution of the turnover frequency

Figure 5.5 presents the variations of the fitted turnover frequencies for C3, C4, C5, and D, which all appear to be correlated. We note that:

1) The evolution of the core spectrum is closely related to the appearance of new superluminal components in the jet. The turnover frequency of the core spectrum increases significantly when a new component is emerging. The rise near 1991.7 corresponds to the appearance of the new feature, C7 (not shown in Figure 5.5).

2) The single antenna observations show sharp rises of the source flux at higher frequencies that are perhaps correlated with the beginning of a new outburst (cf. Teräsranta *et al.* 1992). Such behavior has been interpreted within the shock–in–jet model model (Marscher 1991, Valtaoja *et al.* 1992) which assumes that the high–frequency emission comes from relativistic shocks propagating down the jet. The VLBI data indicate that the core spectrum peaks at higher frequencies than the jet component spectra. Given that the core emission dominates the total flux, the

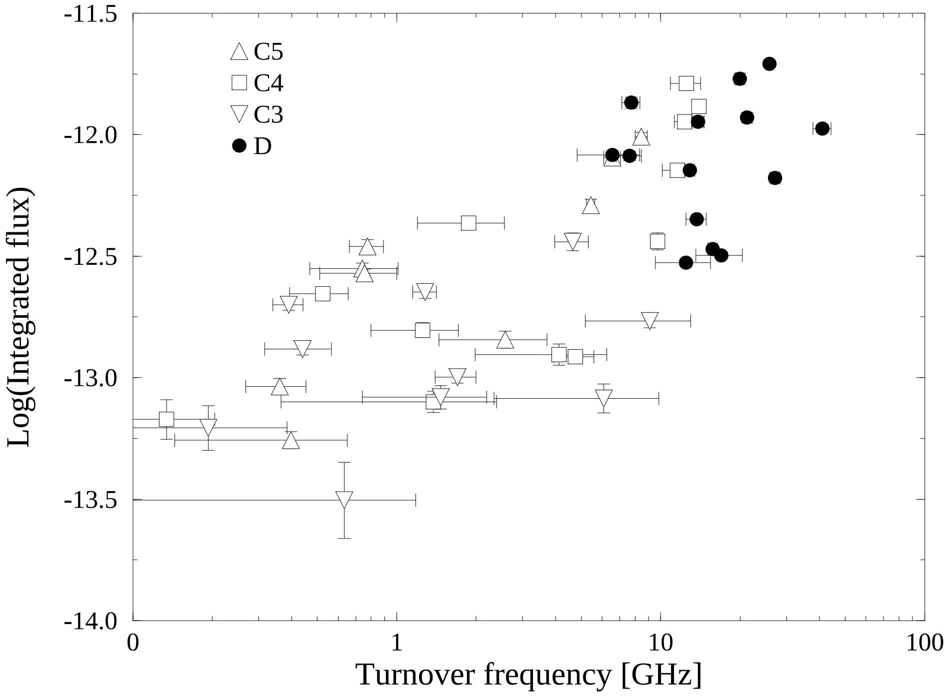

Figure 5.6: Correlation between the integrated 4-25 GHz flux, S_{int}, and turnover frequency, ν_m, of the core , C5, and C4. The integrated flux units are erg $s^{-1}\,cm^{-2}$.

"shock–in–jet" model cannot be easily applied to the jet components (see Chapter 6).

3) C4 and C5 have similar lower turnover frequencies in early stages of their evolution (the spectrum of C3 had already undergone significant changes before 1979, and it is not possible to deduce whether it had peaked at some earlier epoch). These turnover frequencies increase for several years, and then decline steadily until they become relatively stable below 5 GHz.

4) C3, the oldest of the three components, is an example for the late stages of the turnover frequency evolution. The turnover frequency changes weakly with increasing distance from the core and declining component flux, perhaps indicating the presence of physical processes compensating energy losses along the jet. However, the spectral fits may as well be biased against lower values of the turnover frequency.

5.3.2 Turnover frequency and integrated 4–25 GHz flux

In Figure 5.6, we plot the relationship between the integrated 4–25 GHz flux and turnover frequency. For now, we ignore differential Doppler boosting (cf. Kellermann 1994) and changing kinematical parameters along the jet. Overall, the turnover frequency increases with integrated flux. The core (solid circles) retains its spectral maximum at high frequencies during the entire monitoring period ($\nu_m \approx 6.6$–41.0 GHz). Its integrated flux dominates the VLBI emission and does not change significantly.

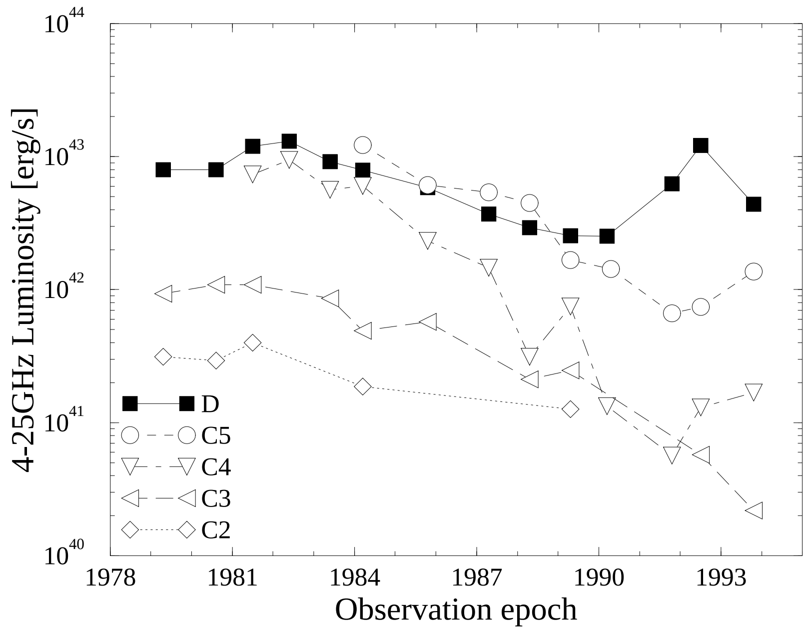

Figure 5.7: 4–25 GHz luminosity evolution of the VLBI core and the jet components in 3C345.

The superluminal components show variations of both turnover frequency and integrated flux. For instance, for C5, ν_m varies from 360 MHz to 8.5 GHz. The integrated flux of C4 changes from 0.7×10^{-13} to 16.2×10^{-13} erg s^{-1} cm^{-2}. The jet components, near the epochs of their maxima, have spectra and fluxes similar to those of the core. The core and the jet components, however, differ in the amplitudes of the spectral variations. The relative stability of the core can be explained by continuous injection of an ultra–relativistic plasma. The "true" core may also be blended, for most of the time, with a close and bright shock, or even with a receding component.

5.3.3 Luminosity and kinematics

We now consider the component luminosities that can be derived from the spectra and their relation to the jet geometry and kinematics. We use the polynomial fits obtained in Chapter 3 for the component trajectories. The luminosities are corrected for the relativistic anisotropy. We use the measured apparent velocity β_{app} and estimate the minimum Lorentz factor $\gamma_{min} = (1 + \beta_{app}^2)^{1/2}$ (Pearson & Zensus 1987) that can produce the observed apparent velocity. Then, we can estimate the upper limit for the 4–25 GHz luminosity

$$L_{4-25GHz} \approx \frac{8\pi c^2 S_{int}}{H_0^2} \left[1 - \cos\left(\frac{1}{\gamma_{min}}\right)\right] \left[1 + z - \sqrt{1+z}\right]^2 . \qquad (5.1)$$

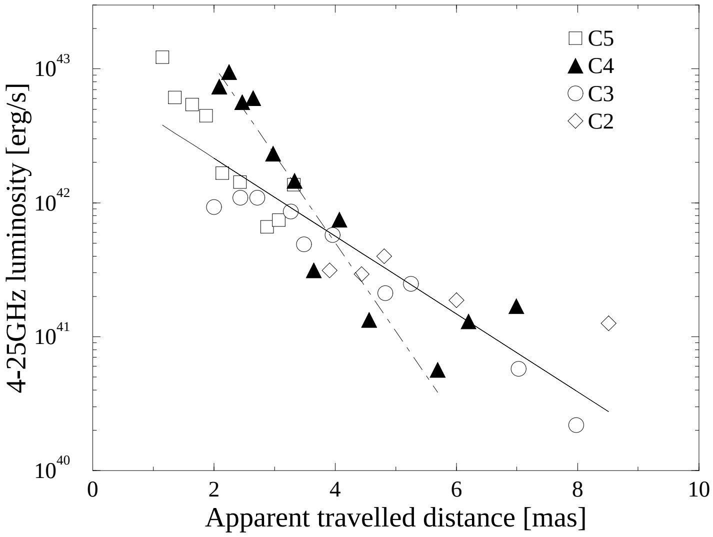

Figure 5.8: Correlation between the components luminosity and apparent distance travelled along the jet. The dot–dashed line is a linear fit to C4 data; the solid line represents the correlation for C2, C3, and C5 data combined.

Table 5.1: Luminosity evolution in parsec–scale features of 3C345

Component	$\log[L_{4-25\,GHz}(t)]$	Comment
D	$43.360 - 0.091\tau$	1981–88
C5	$43.695 - 0.128\tau$	
C4	$43.517 - 0.182\tau$	
C3	$42.280 - 0.110\tau$	
C2	$41.568 - 0.045\tau$	

Notes: $\tau = t - 1979.0\,$[years], where t is current epoch.

Table 5.2: Correlation between the component luminosity and kinematics

Component	$\log[L_{4-25\,GHz}(R_{app})]$	$\log[L_{4-25\,GHz}(R_j)]$ γ =const	$\log[L_{4-25\,GHz}(R_j)]$ $\gamma=\gamma_{min}(t)$
C5	$43.548-0.326\,R_{app}$	$43.323-0.654\,R_j$	$43.534-0.668\,R_j$
C4	$43.346-0.661\,R_{app}$	$41.987-0.027\,R_j$	$43.423-0.945\,R_j$
C3	$42.756-0.286\,R_{app}$	$41.221-0.018\,R_j$	$42.609-0.567\,R_j$
C2	$41.932-0.100\,R_{app}$	$41.220-0.011\,R_j$	$42.067-0.234\,R_j$
All	$42.914-0.290\,R_{app}$	$42.060-0.030\,R_j$	$43.066-0.638\,R_j$

The derived luminosities and minimum Lorentz factors are given in Table 4.7 in Chapter 4. Figure 5.7 shows the component luminosity evolution. We estimate $\gamma \approx 3.5$ for the core, assuming that the Lorentz factor of the core is similar to the initial Lorentz factors of the moving components (ZCU95). This yields $L_D = (7.1 \pm 3.5) \times 10^{42} h^{-2}\,\mathrm{erg\,s^{-1}}$ for the average luminosity of the core. We estimate the total 4–25 GHz luminosity of the jet features $L_{jet} \approx 3 \times 10^{43} h^{-2}\,\mathrm{erg\,s^{-1}}$ which amounts to about 1% of the observed radio–through–infrared luminosity of 3C345 (Bregman *et al.* 1986). The luminosities of all components, with the exception of C2, decrease at approximately the same rate of $1.2 \times 10^{35} h^{-2}\,(0.74 \pm 0.06)^{t-1979.0}\,\mathrm{erg\,s^{-2}}$ (for D, we determined the decrease rate for the epochs between 1981 and 1988). The derived decrease rates are given in Table 5.1. Comparable rates of energy loss in different jet components may indicate similar emission mechanisms. The only exception to the observed similarity is the luminosity of C4 which decreases almost twice as fast compared to D, C3, and C5. This difference can be explained by several factors:

1) Because of the narrow frequency range, the observed dependencies might not reflect physical conditions in the jet adequately. Therefore, the observed similarities might be coincidental. However, most of the observed spectra have their maxima within 4–25 GHz, so their evolutions must be similar in order to produce comparable rates of luminosity decrease.

2) It is possible that our analysis underestimated the Lorentz factors of the components C2, C3, and C5. However, it would require very high Lorentz factors of C3 and C5, to match the slope of C4. Such a scenario would yield, in 1988, $\gamma_{C5} \approx 26$ and $\gamma_{C3} \approx 35$, which is considerably higher than the theoretical limits on the bulk Lorentz factor expected in a jet ($\gamma \approx 20$; Abramovicz 1992; Henri and Pelletier 1992).

3) C4 might represent a composition of two possibly related features in the jet. The observations made in 1984–86 indicate that C4 could be a blend of two emitting regions (ZCU95). A compound nature of C4 is not self–evident at later epochs, and we suggest that the emission from any weaker subcomponent was completely indistinguishable from the stronger and faster counterpart (C6 and C7 may represent a similar situation: a faster component overtaking an older and slower feature; Zensus *et al.* 1995b). This might result in an increase of the measured proper motion and,

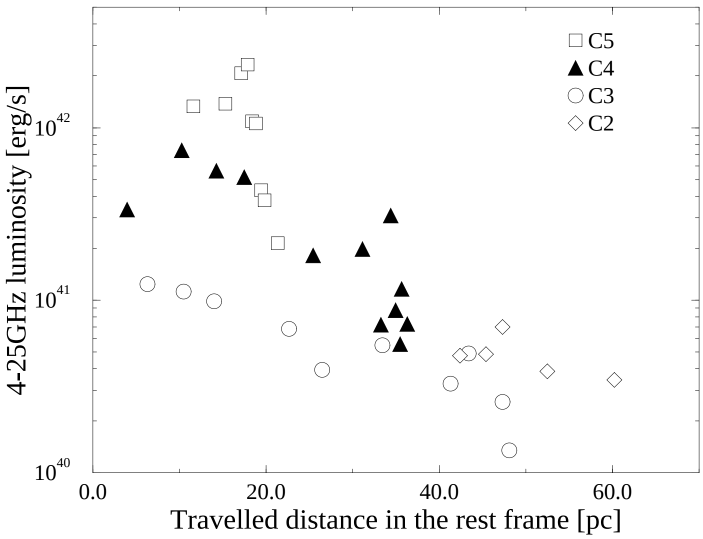

Figure 5.9: Correlation between the components luminosity and distance travelled in the rest frame of the jet. The components move at constant speed. The Lorentz factors $\gamma_{C2,3} = 20$, and $\gamma_{C5} = 7$, $\gamma_{C4} = 15$ are chosen so as to provide consistency of the component kinematic evolutions in the jet rest frame.

correspondingly, in higher values of γ_{min}. At the same time, C4 may indeed be different from the other jet features, and the difference could be due to physical factors, rather than to the jet geometry.

Figure 5.8 presents correlations between the derived component luminosities and the apparent distance travelled along the jet

$$R_{app}(t) = \int_0^t \mu(t)\,\mathrm{d}t\,,$$

where $\mu(t)$ is component proper motion, and $t = 0$ corresponds to the component epoch of origin. Again, the luminosities of C2, C3, and C5 depend on R_{app} in a similar fashion, so that it is possible to find a general trend over the jet length up to 8 mas distance from the core. The linear fit shown in Figure 5.8 as a solid line corresponds to $\log(L_{C2,3,5}) = 42.91 - 0.29\,R_{app}$. The same procedure applied to C4 yields $\log(L_{C4}) = 44.35 - 0.66\,R_{app}$. All fits are given in Table 5.2.

In order to study the luminosity evolution in the rest frame of the jet, certain assumptions must be made about the component kinematics. Below, we consider the luminosity evolution in two cases: a) a curved jet moving with constant speed, and b) an accelerating jet satisfying the minimum kinetic power condition $\gamma = (1 + \beta_{app})^{1/2}$. The distance travelled by a component in the rest frame of the jet is

$$R_j(t) = \int_0^t \varphi(z, \vec{\beta})\,\beta\,\mathrm{d}t\,,$$

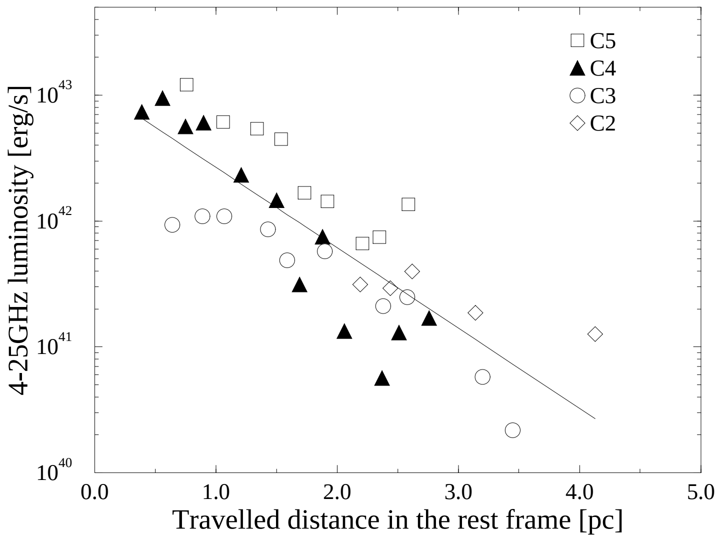

Figure 5.10: Correlation between the component luminosity and travelled distance in the rest frame of the jet. The jet moves with $\gamma = \gamma_{min}(t)$. The solid line represents a fit to the total data.

where φ accounts for time shortening in the observer's frame, and the component velocity $\vec{\beta}$ varies with time.

In Figure 5.9, we plot the luminosity evolution in a constant–velocity jet. Due to kinematic constraints, the component Lorentz factors must differ significantly: $\gamma_{C5} = 7$, $\gamma_{C4} = 15$, $\gamma_{C3,C2} = 20$. Even so, the components are not well correlated (see Table 5.2): at comparable distances, the luminosities can be different by more than one order of magnitude. C5 also shows a much steeper decrease of its luminosity compared to the other components. Such discrepancies suggest that the component intrinsic velocities may vary along the jet. One of the possible cases of variable component velocities is shown in Figure 5.10. The variations of the component Lorentz factors are such that they provide the least distance travelled in the jet rest frame. The solid line in Figure 5.10 shows the luminosity evolution $\log(L_{jet}) \approx 42.06 - 0.03\, R_j$ derived for all the components. With exception of C2 (for which the luminosity calculations are not reliable), the individual component evolutions do not deviate significantly from the overall trend (see Table 5.2). The derived correlations suggest that, if the physical conditions of the jet components are similar, then intrinsic accelerations are required for explaining the changes in component luminosities.

5.4 Summary

The main results of this chapter can be summarized as follows:

1) Flux curves of the core and C7 show a possible signature of delayed maximum

flux at lower frequencies, with respect to higher frequencies. No such delays are observed in the flux curves of C4 and C5 which both reached their maxima at larger separations from the core, compared to C7. This fact can argue that the delay of maximum flux can be related to changing opacity along the jet, and affect the emission within $\leq$1 mas separations from the core.

2) Flux evolutions of the strong jet components are similar. After achieving the maximum flux, the component show $\approx$ 15% a year decrease. Later the decrease becomes slower ($\approx$ 5% a year). The weak jet features have peculiar flux evolution characterized by sudden drops of the flux (C5), and extremely low 22 GHz flux (C6). The peculiarity of the flux changes observed in C5 and C6 can be related to their unusual kinematical parameters.

3) Correlation between the turnover frequency and integrated 4–25 GHz flux is observed in the core and the jet components. The core integrated flux dominates the emission, at most of the epochs. Both the turnover frequency and integrated flux of the core vary within smaller ranges compared to the changes observed in the jet components. Continuous injection of ultra–relativistic plasma, or blending with the closest shocked feature may explain the observed relative stability of the core spectral properties.

4) Evolutions of the turnover frequencies of the core and the jet component are correlated. The turnover frequency of the core rises, with appearance of a new superluminal feature. The jet components, C4 and C5, have peaked evolutions of the turnover frequency.

5) Luminosities of the core and the jet features decrease at approximately the same rate. C4 experiences a change of the decrease rate, between 1984 and 1988. No jet model with constant velocity can account for the observed change of the decrease rate. The most likely explanations are the acceleration of C4, or possible split of the component into two superluminal features.